Analyses of Local Open Circuit Voltages in Polycrystalline Cu(In,Ga)Se$_2$ Thin Film Solar Cell Absorbers on the Micrometer Scale by Confocal Luminescence

Gottfried Heinrich Bauer* and Levent Gütay

Abstract: Polycrystalline chalcopyrite absorbers in thin film solar cells exhibit distinct spatial inhomogeneities which are obviously introduced during growth of the grainy structure. Amongst several structural inhomogeneities in scale lengths of grains of one µm or below, spatial variations of optoelectronic properties in much larger scales of some µm can be observed, such as fluctuations in the splitting of quasi-Fermi levels in the range of several tens of meV. These have been quantitatively deduced *via* Planck's generalized law from spectrally resolved confocal room temperature luminescence scans. Since the necessary absorption length in thin film semiconductors is in the neighborhood of the wavelength of photons, for the evaluation of luminescence spectra wave optics with multi-reflection effects have been applied.

Keywords: Chemical potential of electron–hole ensembles · Confocal photoluminescence · Cu(In,Ga)Se$_2$ · Thin film solar cells

Introduction

Polycrystalline chalcopyrite absorbers such as Cu(In,Ga)Se$_2$ (CIGSe) have attracted extreme attention by displaying world record solar light conversion efficiencies for thin film lab cells in the neighborhood of 20%.[1] However due to the polycrystalline nature of the absorber with grain sizes in the µm-scale and below considerable inhomogeneities, like spatial fluctuations of grain size and orientation, as well as elemental composition of grains and related variations of optical and electronic properties occur and have been observed by various methods.[2–14] Because of these spatial fluctuations of semiconductor properties, local variations *e.g.* in photo carrier generation and in carrier life times have to be expected, which result in local fluctuations of excess carrier concentrations governing the local quality of the photoexcited state.

Theoretical Background

We analyze the state of such absorbers under illumination by the emitted light and we formulate the photon flux $\Gamma(\omega)$ according to Planck's generalized law[15–18] which writes for a volume element

$$\Gamma(\omega) \propto \varepsilon(\omega) \frac{\omega^2}{\left\{ \exp[\frac{\hbar\omega - \mu_{phot}}{kT}] - 1 \right\}} d\Omega \quad (1)$$

where $\varepsilon(\omega)$, $\hbar\omega$, μ_{phot}, kT designate spectral emissivity, photon energy, chemical potential of the photon field, and thermal energy; the denominator represents the Bose-term (see Fig. 1).

Provided energy and momentum relaxation times of photoexcited electrons in the conduction band and holes in the valence band are small compared to the transition times of carriers to the ground state, explicitly the recombination life time, the distribution of carriers can be described by the quasi-Fermi approach and the chemical potential of the photon field equals the chemical potential of the electron–hole ensemble representing the splitting of the quasi-Fermi levels ($\varepsilon_{Fn}-\varepsilon_{Fp}$). In inorganic semiconductors with a minimum degree of suitability for light conversion this requirement is necessarily satisfied; if not, the eventual efficiency of those devices is negligible.

For the formulation of the emission of luminescence photons from a particular depth z in the absorber in terms of the spectral photon flux $\Gamma_{Det}(\omega,z)$ (see Eqn. (2)) we introduce multi-reflection effects by the energy dependent (one-dimensional) propagation of photons back and forth and across interfaces in the respective film sequences, *e.g.* substrate/absorber/window layer. We apply a matrix transfer formalism with complex refractive indices and calculate the luminescence photon flux towards the detector for different depth profiles of the luminescence that is created by radiative recombination of respective carrier distributions. Spectral absorption and refractive indices are taken from local spectral luminescence and transmission analyses.[19]

Correspondence: Prof. Dr. G. H. Bauer
Institute of Physics
Faculty of Mathematics and Natural Sciences
Carl von Ossietzky University
D-26111-Oldenburg, Germany
Tel.: +49 441 798 3498
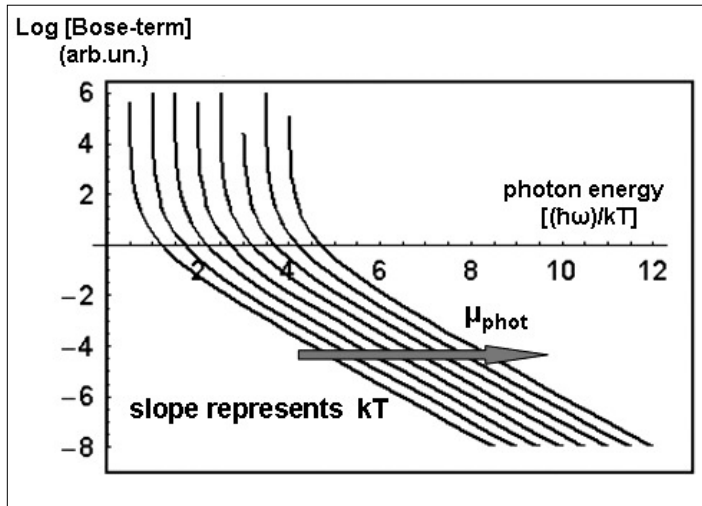Fax: +49 441 798 3201
E-Mail: g.h.bauer@uni-oldenburg.de

Fig. 1. Calculated Bose-term versus photon energy governing the emission from matter in different excitation states (different chemical potentials μ_{phot}); for sufficiently high photon energies, for which the absorption $A \approx 1$, this term governs the spectral luminescence in terms of temperature (slope in the log-plot) and of chemical potential (vertical shift of the spectra).

$$\Gamma_{Det}(\omega,z) \propto \varepsilon(\omega)\frac{1}{4}(t_{12})^2 \Gamma_{phot}(z)\exp(-2\alpha(d-z)) \left| \frac{1+2r_{10}\exp(-2\alpha z)\exp[i2kz]+(r_{10})^2\exp(-4\alpha z)}{1-2r_{01}r_{12}\exp(-2\alpha d)\exp[i2kd]+(r_{01}r_{12})^2\exp(-4\alpha d)} \right|^2 \omega^3 \left[\exp[\frac{\hbar\omega-\mu_{n,p}}{kT}]-1 \right]^{-1}$$

(2)

Here t_{ij}, and r_{ij} are amplitude transmission and reflection coefficients determined by particular refraction indices; α, d, and k designate amplitude attenuation coefficient, thickness of the absorber, and photon wave vector therein; $\Gamma_{phot}(z)$ represents the local photon emission, with 0.5 $\Gamma_{phot}(z)$ propagating to the right and $\Gamma_{phot}(z)$ to the left hand side; the influence of the (60–70) nm thick CdS window layer on the optical properties in this approach due to effective medium theory has been neglected.

Experimental Results and Interpretation of Data

We analyze the luminescence from layer sequences Mo/Cu(In$_x$Ga$_{1-x}$)Se$_2$/CdS or glass/Cu(In$_x$Ga$_{1-x}$)Se$_2$/CdS in a confocal setup described in detail elsewhere[20] with the particular feature of a reflection microscope objective for wavelength independent focusing of the incoming laser beam ($\lambda = 633$ nm) onto the sample as well as for the collection of emitted luminescence light ($\lambda \approx 1$ μm) in an optical multi-channel detector. An entire spectrum is recorded for each local position within the scan of *e.g.* (50 μm)^2. The samples are taken from runs with reasonably high solar cell efficiencies of $\eta \approx 16\%$.[21]

Fig. 2 displays (50 μm)^2 scans of the afm-topology of Cu(In$_{0.7}$Ga$_{0.3}$)Se$_2$ (on Mo-coated glass substrate) (Fig. 2a) and pl-yields recorded for different laser excitation fluxes. With a lateral resolution of our setup close to the diffraction limit of about

1 μm or less, we observe substantial pattern sizes of pl-yields of some microns whereas the afm-picture qualitatively represents the morphological feature of the grain sizes in the scale of ≤1 μm. The origin of the pl-pattern, which is considerably larger than grain sizes, is not entirely clear; there is strong evidence for spatially varying elemental composition of the absorber which results in local fluctuations of optical band gaps, for laterally fluctuating carrier diffusion, and also for local variations of the electronic environment (high or low resistive contacts to neighbor grains/sites).[22,23] Luminescence scans of absorbers on Mo and on glass substrates show comparable lateral variations in pl-yield and spectral distribution and these features are also observed regardless of the direction of recording, *e.g.* from top (rough surface) or from bottom through the glass substrate (flat surface). From that and from the pattern sizes we conclude the pl-features to be mainly governed by bulk properties and not by light scattering at the rough front surface.

As a consequence of the extremely small area probed with the confocal setup (<0.8 μm^2) the luminescence photon flux as response to the excitation with one sun-equivalent photon fluxes (3×10^{17} cm^{-2}s^{-1}) – particularly at 300 K where the fraction of radiative recombination is below 10^{-2}[22] – is too low to be detected properly (<10^7 photons/s). We thus have excited at higher photon fluxes and extrapolate our results towards one sun-excitation and adjust them to pl-analyses of larger areas without lateral resolution.[24]

The dependence of the pl-patterns on excitation laser flux (compare Figs 2b and 2c) can be explained consistently in terms of nonlinear kinetics for radiative recombination (superlinear behavior of radiative recombination versus excess carrier density) and with simultaneous lateral excess carrier diffusion.[22] Note that the amplitudes of the fluctuations of the pl-yield substantially increase for decreasing excitation.
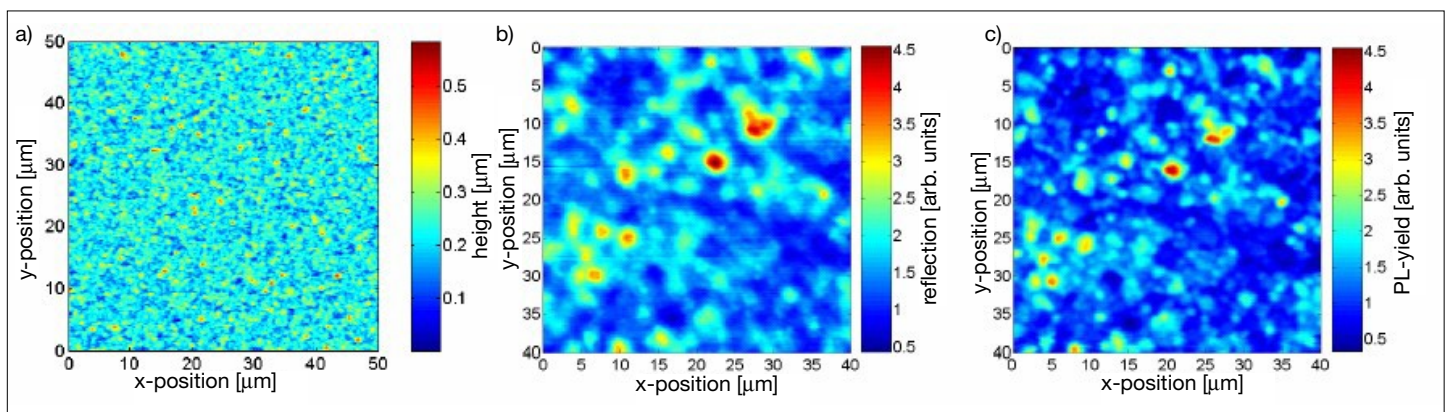

Fig. 2. Lateral scans ((50 μm)^2) of a Cu(In$_{0.7}$Ga$_{0.3}$)Se$_2$ absorber in a Mo/CIGSe/CdS-structure; afm-height distribution which shows the rough topology of the film resulting from individual grains (left), room temperature luminescence yields at different excitation fluxes $\Phi_0 = 3 \times 10^4$ suns equivalent (center), and $10^{-2} \Phi_0$ (right) as an indication of fluctuations of the optoelectronic properties.
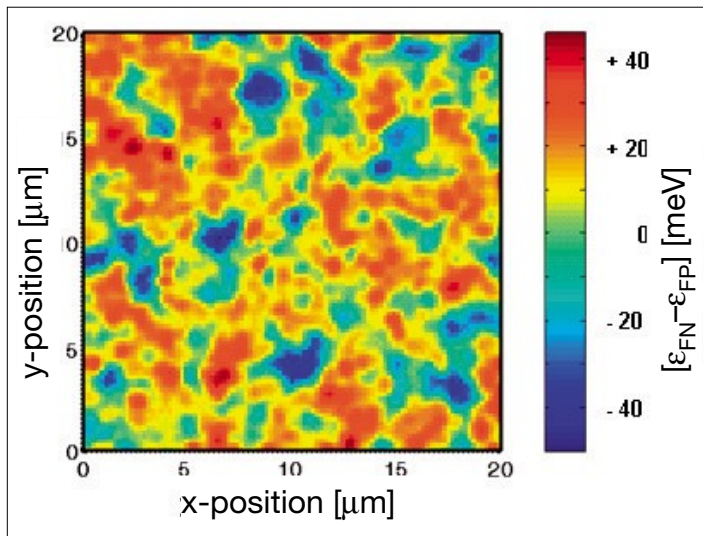
Fig. 3. Lateral fluctuations of room temperature quasi-Fermi level splitting $\Delta(\varepsilon_{Fn}-\varepsilon_{Fp})$ in a $Cu(In_{0.7}Ga_{0.3})Se_2$ absorber sandwiched between a Mo rear contact and 70 nm thick CdS window (excitation by 3×10^4 sun-equivalent photon fluxes); the center value of the splitting $(\varepsilon_{Fn}-\varepsilon_{Fp})$ here amounts to about 910 meV.

From the spectrally resolved lateral luminescence yields of scans shown *e.g.* in Figs 2b and 2c we deduce local fluctuation of quasi-Fermi levels outlined in Fig. 3. These spatial fluctuations have been evaluated from spectra at each scan position and at photon energies $\hbar\omega^*$ where almost complete absorption/emissivity $(A(\omega^*) = \varepsilon(\omega^*) \approx 1)$ is achieved (see Eqn. (3)) and with the approximation that the refractive index contrast between the different local sites for coupling laser photons in and coupling luminescence photon out is comparably small (in the low percentage range). Consequently, lateral fluctuations of the pl-yields amounting to a factor of up to ten, almost exclusively result from laterally varying bulk properties of the absorber, *e.g.* carrier concentrations.

$$\Delta(\varepsilon_{Fn} - \varepsilon_{Fp}) = kT \ln\left[\frac{Y_{pl}(x_i, \omega^*)}{Y_{pl}(x_j, \omega^*)}\right] \quad (3)$$

In Fig. 4 we present a histogram of local fluctuations $\Delta(\varepsilon_{Fn}-\varepsilon_{Fp})$ of the data of Fig. 3 with a typical half width (FWHM) of 20–30 meV. We would like to emphasize that the fluctuations of pl-yields and accordingly those of the Fermi-level splitting become even more pronounced when reducing the excitation towards AM1-equivalent photon fluxes (see Figs 2b, 2c and ref. [24]).

Numbers for the total splitting of the quasi-Fermi levels $(\varepsilon_{Fn}-\varepsilon_{Fp})$ in addition to their local fluctuations $\Delta(\varepsilon_{Fn}-\varepsilon_{Fp})$ have been derived by

i) averaging (summing up) the laterally resolved spectra $([\Sigma Y_{PL,i}])$,

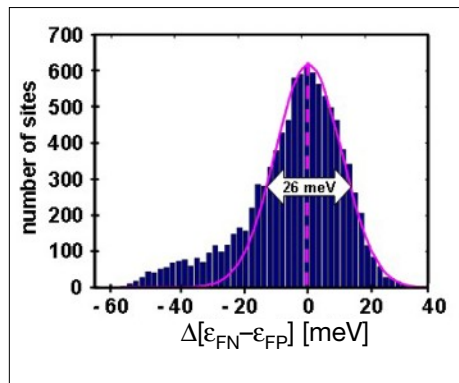ii) comparing these 'averaged' spectra with those experimentally recorded from large areas (1 mm^2) for which we

Fig. 4. Histogram of fluctuations of the quasi-Fermi level $\Delta(\varepsilon_{Fn}-\varepsilon_{Fp})$ in a $Cu(In_{0.7}Ga_{0.3})Se_2$ absorber (data from Fig. 3).

can record calibrated values for photon fluxes and according to Fermi level splitting,[18,25] which yield the 'incorrect' value

$$(\varepsilon_{Fn}-\varepsilon_{Fp})_{incorr.} \sim kT \ln [\Sigma Y_{PL,i}] \quad (4a)$$

iii) and finally correcting with the distribution of the histogram for the correct value

$$(\varepsilon_{Fn}-\varepsilon_{Fp})_{corr.} \sim kT (\Sigma \ln[Y_{PL,i}]) \quad (4b)$$

Neglecting the above discrepancy we estimate an average of $(\varepsilon_{Fn}-\varepsilon_{Fp})_{incorr.} \approx$ 910 meV. The difference between 'correct' (Eqn. (4b)) and 'incorrect' averaging (Eqn. (4a)) has been calculated for our data and amounts to $\Delta\varepsilon_{wrong,av} \leq -5$ meV, which means that the correct average splitting of the quasi-Fermi levels (center value *e.g.* in Fig. 3) is smaller by at least 5 meV.

The extraction of the chemical potential $(\varepsilon_{Fn}-\varepsilon_{Fp})$ of the electron–hole ensemble and its lateral fluctuation from experimental luminescence data strongly needs the detailed knowledge of the depth position where photons are generated, and on their propagation to the detector through the involved layer structure. The propagation terms of course have to include attenuation by absorption, reflection at phase borders, and interference effects (see Eqn. (2)). We have calculated spectral pl-yields arriving at the detector for different exemplary depth profiles of the luminescence (excess carrier concentrations) in which actual local values for refractive indices, layer thicknesses and absorption coefficients have been introduced from previous work[19] (Figs 5a,b and 6a,b). The Figs show calculated luminescence signals firstly for depth profiles extending more and more from the rear contact towards the front side of the absorber (Figs 5a, b) and secondly for profiles extending from the front side (CdS-window) more and more towards rear contact (Figs 6a, b).

In the spectra, the spectral absorption $A(\omega)$ and the absorption coefficient $\alpha(\omega)$ is most significantly reflected in the low energy wing of the spectral luminescence where $A(\omega) = (1-\exp[-\alpha(\omega)d]) << 1$, which means $A(\omega)$ is sufficiently small. Here the influence of the type of depth profile on the signal of the pl-detection is considerably strong.

The negative slope in the log-plot of the high energy pl-wing – of course, corrected by $1/(\omega^2)$ – indicates the local temperature.

The actual values of the chemical potential $\mu_{phot} = (\varepsilon_{Fn}-\varepsilon_{Fp})$ shifts the entire function in direction of the ordinate axis. Thus for the deduction of $(\varepsilon_{Fn}-\varepsilon_{Fp})$ we use the regime of the high energy wing, where interference effects disappear.

Figs 5b and 6b demonstrate the strong impact of interference effects in these layer structures and in particular reveal the influence of re-absorption of high energy luminescence photons. In our analyses (for CIGSe) due to the comparatively low ratio of radiative to non-radiative recombination rates $r_{rad.}/r_{non-rad.} < 10^{-2}$ photon recycling [22] at 300 K needs not be considered.

Re-absorption is certainly negligible for the emission from the position next to the border of the absorber oriented in direction to the detector (Fig. 6b), and in this configuration the values of the recorded pl-signal of the high energy wing are marginally modified by luminescence contributions from additional layers at larger depths.

In our case the electronically sufficiently thick CdS window layer (dCdS $\approx$ 50 nm) can be assumed to efficiently passivate surface states of $Cu(In_{1-x}Ga_x)Se_2$ at least for x $\leq$ 0.5 and this electronically thick layer is still optically thin and consequently its effect on photon propagation is negligible. In CIGSe-heterodiodes the electronic junction is
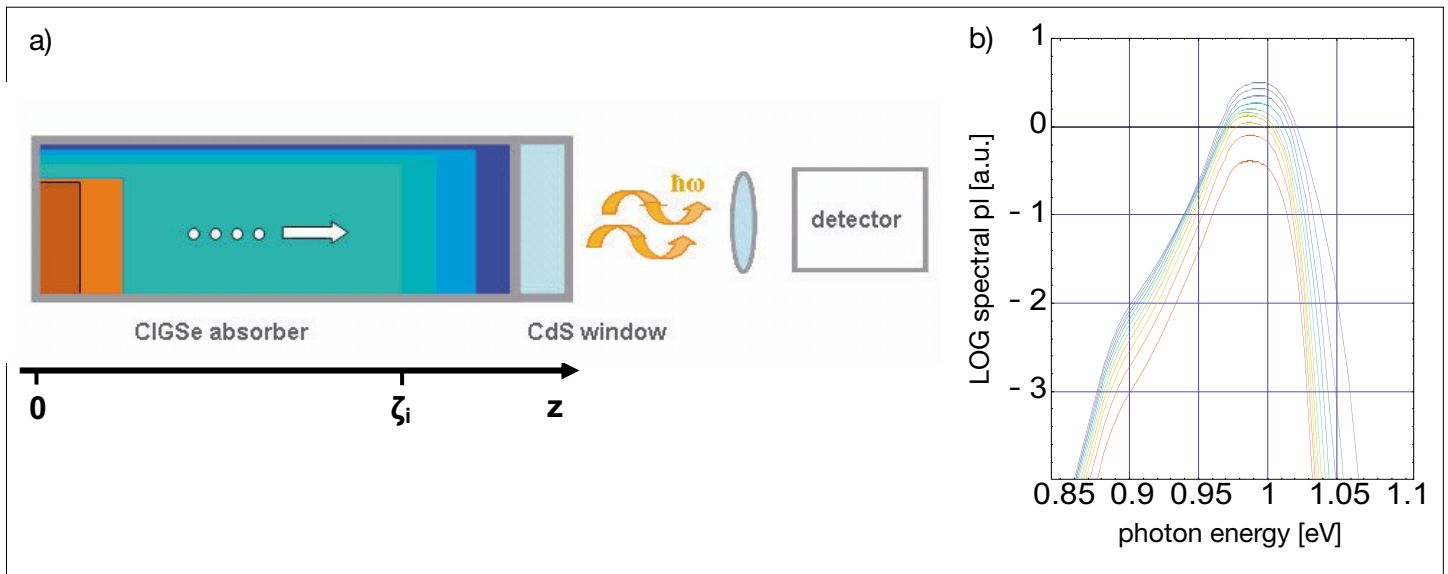
Fig. 5a,b. Exemplary depth profiles of luminescence (excess carrier concentration) (left part) with thickness extending from the rear contact ($\varsigma = 0$) more and more towards the front window layer ($0 \leq \varsigma \leq d$), and according calculated spectral luminescence yield transferred to the detector (right part), note, low and high energy wings are strongly dependent on type of profile.
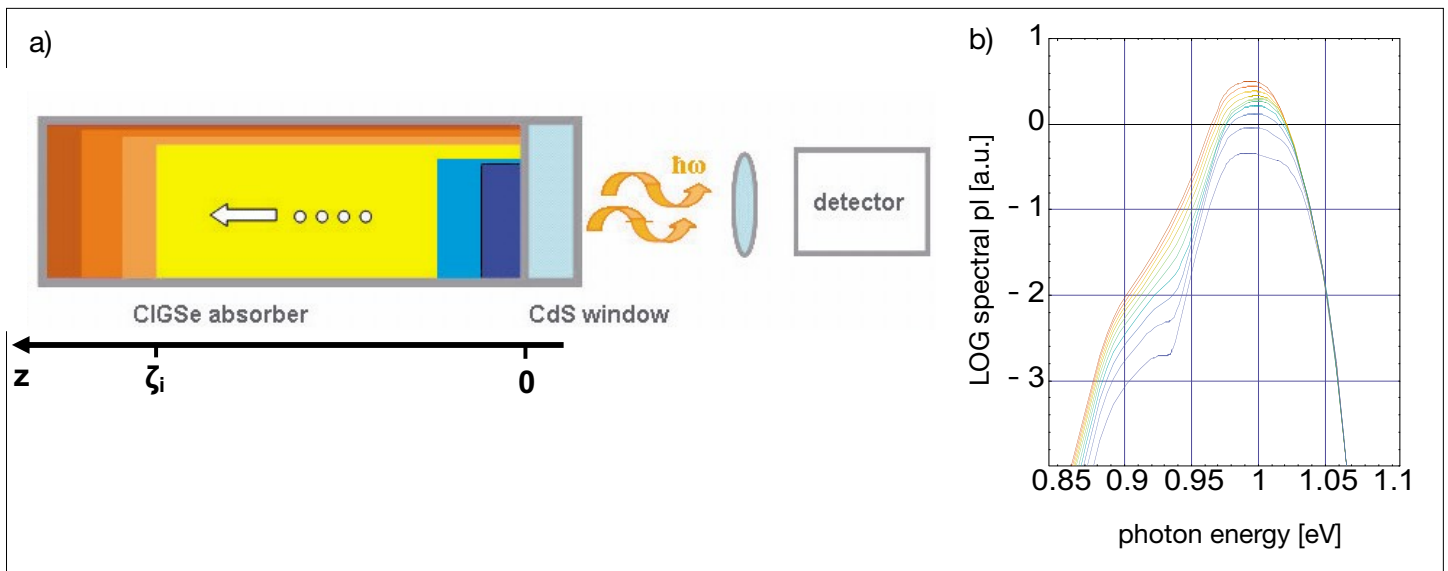

Fig. 6a,b. Exemplary depth profiles of luminescence (excess carrier concentration) (left part) with thickness extending from the front window layer ($V = 0$) more and more towards the rear contact ($0 \leq V \leq d$), and according calculated luminescence yield transferred to the detector (right part), note, at variance with the situation in Figs 5a, b the high energy wing is unaffected by an extension of the profile deeper into the absorber.

formed by the CIGSe/CdS-interface which represents the entrance side of the sunlight, as well as the direction of our laser excitation, and thus we may justifiably attribute the ($\varepsilon_{Fn}-\varepsilon_{Fp}$) experimentally analyzed by luminescence studies from the CdS-window-side (Fig. 6) directly to the splitting of the Fermi levels ($\varepsilon_{Fn}-\varepsilon_{Fp}$) at the heterojunction CIGSe/CdS; the spatial average of this magnitude ($\varepsilon_{Fn}-\varepsilon_{Fp}$) represents, with good approximation, the maximum achievable open circuit voltage of a final device.

Conclusions

In polycrystalline chalcopyrite absorbers like Cu(InGa)Se$_2$ which have been proven by outstanding light conversion performances, the growth of the absorber obviously implies a considerable local fluctuation of the quality of the photogenerated excitation state, which is generally related to the grainy structure and its inhomogeneity, but shows additional lateral features larger than grain sizes. As the mixing of parameters governing this state in terms of thermodynamics represents a mixture of intense variables which is always accompanied by a reduction of the free energy of the respective ensemble, here the excited electrons and holes, the output of those devices would even be higher if the local inhomogeneities could be reduced or avoided.

Our confocal setup allows the detection of lateral optoelectronic inhomogeneities on the one-micron scale, however, we cannot exclude contributions to inhomogeneity effects resulting from smaller lengths scales.[19]

Due to non-linear superposition of local properties to values averaged over particular areas, we have to recognize that the interpretation of any experiment with insufficient spatial resolution and the subsequent extraction of data will in principle not show the correct features.

[1] K. Ramanathan, M. Contreras, C. L. Perkins, S. Asher, F. S. Hasoon, J. Keane, D. Young, M. Romero, W. Metzger, R. Noufi, J. Ward, A. Duda, *Prog. Photovolt.: Res. Appl.* **2003**, *11*, 225.

[2] D. Eich, U. Herber, U. Groh, U. Stahl, C. Heske, M. Marsi, M. Kiskinova, W. Riedl, R. Fink, E. Umbach, *Thin Solid Films* **2000**, *258*, 361.

[3] N. G. Dhere, S. R. Ghonadi, M. B. Pandit, A. A. Kadam, A. H. Jahagirdar, V. S. Gade, 'Conf. Rec. 29 IEEE Photovolt. Spec. Conf.', Ed. J. Benner, IEEE, Piscataway, **2002**, p. 876.

[4] C.-S. Jiang, R. Noufi, J. A. AbuShama, K. Ramanathan, H. R. Moutinho, J. Pankow, M. M. Al-Jassim, *Appl. Phys. Lett.* **2004**, *84*, 3477.

[5] D. F. Marron, S. Sadewasser, A. Meeder, T. Glatzel, M.C. Lux-Steiner, *Phys. Rev. B* **2005**, *71*, 033306.

[6] G. Hanna, T. Glatzel, S. Sadewasser, S. Schuler, S. Nishiwaki, R. Kaigawa, C.-M. Lux-Steiner, *Thin Solid Films* **2003**, *257*, 431.

[7] N. Ott, G. Hanna, U. Rau, J. Werner, H. P. Strunk, *J. Phys.: Cond. Mat.* **2004**, *16*, 85.

[8] K. Bothe, G. H. Bauer, T. Unold, *Thin Solid Films* **2001**, *405*, 453.

[9] M. J. Romero, K. Ramanathan, M. A. Contreras, M. M. Al-Jassim, R. Noufi, *Appl. Phys. Lett.* **2003**, *83*, 4770.

[10] Y. Yanfa, R. Noufi, K. M. Jones, K. Ramanathan, M. M. Al-Jassim, *Appl. Phys. Lett.* **2005**, *83*, 121904.

[11] S. Sadewasser, *Thin Solid Films* **2006**, *515*, 6136.

[12] S. Siebentritt, T. Eisenbarth, M. Wimmer, C. Leendertz, F. Streicher, S. Sadewasser, M. Lux-Steiner, *Thin Solid Films* **2006**, *515*, 6168.

[13] G. H. Bauer, L. Gütay, R. Kniese, *Thin Solid Films* **2005**, *480*, 259.

[14] J. H. Werner, J. Mattheis, U. Rau, *Thin Solid Films* **2005**, *480*, 399.

[15] P. Würfel, 'Physics of Solar Cells', Wiley, Weinheim, **2004**.

[16] K. Schick, E. Daub, S. Finkbeiner, P. Würfel, *Appl. Phys. A* **1992**, *54*, 109.

[17] G. Smestad, H. Ries, *Solar Energy Materials and Solar Cells* **1992**, *25*, 51.

[18] T. Unold, D. Berkhahn, B. Dimmler, G. H. Bauer, in 'Proc. 16 Europ. Photovolt. Sol. Energy Conf.', Eds. H. Scheer *et al.* James & James Science Publ., London, **2000**, p. 737.

[19] L. Gütay, G. H. Bauer, in 'Mater. Res. Soc. Symp. Proc.', **2007**, Vol. 1012, p. Y08-03.

[20] G. H. Bauer, K. Bothe, T. Unold, in 'Conf. Rec. 29 IEEE Photovolt. Spec. Conf.', Ed. J. Benner, IEEE, Piscataway, **2002**, p. 700.

[21] T. Kirchartz, U. Rau, M. Kurth, J. Mattheis, J. H. Werner, *Thin Solid Films* **2006**, *515*, 6238.

[22] G. H. Bauer, L. Gütay, *Thin Solid Films* **2006**, *515*, 6127.

[23] T. Jürgens, L. Gütay, G. H. Bauer, *Thin Solid Films* **2006**, *515*, 678.

[24] G. H. Bauer, L. Gütay, R. Kniese, *Thin Solid Films* **2005**, *480*, 259.

[25] G. H. Bauer, R. Brüggemann, S. Tardon, S. Vignoli, R. Kniese, *Thin Solid Films* **2005**, *480*, 410.